Euler buckling instability and enhanced current blockade in suspended single-electron transistors

Guillaume Weick,[1] Felix von Oppen,[2] and Fabio Pistolesi[3,4]

[1]*Institut de Physique et Chimie des Matériaux de Strasbourg (UMR 7504), CNRS and Université de Strasbourg, 23 rue du Loess, Boîte Postale 43, F-67034 Strasbourg Cedex 2, France*

[2]*Dahlem Center for Complex Quantum Systems & Fachbereich Physik, Freie Universität Berlin, Arnimallee 14, D-14195 Berlin, Germany*

[3]*Centre de Physique Moléculaire Optique et Hertzienne (UMR 5798), CNRS and Université de Bordeaux I, 351 Cours de la Libération, F-33405 Talence Cedex, France*

[4]*Laboratoire de Physique et Modélisation des Milieux Condensés (UMR 5493), CNRS and Université Joseph Fourier, 25 avenue des Martyrs, Boîte Postale 166, F-38042 Grenoble Cedex, France*

(Received 5 October 2010; revised manuscript received 25 November 2010; published 24 January 2011)

Single-electron transistors embedded in a suspended nanobeam or carbon nanotube may exhibit effects originating from the coupling of the electronic degrees of freedom to the mechanical oscillations of the suspended structure. Here, we investigate theoretically the consequences of a capacitive electromechanical interaction when the supporting beam is brought close to the Euler buckling instability by a lateral compressive strain. Our central result is that the low-bias current blockade, originating from the electromechanical coupling for the classical resonator, is strongly enhanced near the Euler instability. We predict that the bias voltage below which transport is blocked increases by orders of magnitude for typical parameters. This mechanism may make the otherwise elusive classical current blockade experimentally observable.

DOI: 10.1103/PhysRevB.83.035420 PACS number(s): 73.63.−b, 85.85.+j, 63.22.Gh

I. INTRODUCTION

Single-electron transistors (SETs) are extremely sensitive devices and are investigated as position detectors for nanoelectromechanical systems (NEMS).[1–3] But the reduced size of the mechanical resonator implies that the backaction of the SET can have significant effects on the mechanical degree of freedom, such as the generation of self-oscillations.[4–6] In practice, the detector and the resonator have to be investigated collectively as a single system. A prominent example of the new effects displayed by this device is the current blockade that appears at low-bias voltage V when the SET is coupled capacitively to a classical oscillator.[7] The physical idea behind this phenomenon is simple: The presence of an extra electron on the central island of the SET induces an additional electrostatic force F_e on the oscillator (see Fig. 1). Thus, the equilibrium position of the oscillator is shifted by a distance F_e/k, where k is the oscillator spring constant. After such a displacement, the gate voltage V_g seen by the SET changes by a quantity of the order of $F_e \times F_e/ek \equiv E_E/e$, where e is the electron charge. The dimension of the conducting window in V_g is controlled by V, since at low temperatures, current can flow through the device only if $|V_g| \lesssim V$ (when measuring V_g from the degeneracy point). Thus, for $eV < E_E$, the fluctuation of the electronic occupation of the central island suffices to bring the device out of the conducting window. The current is blocked for $eV < E_E$, and a mechanical bistability appears.[7] This phenomenon is the classical counterpart of the Franck-Condon blockade in molecular devices[8,9] that has recently been observed in suspended carbon nanotubes for high-energy vibrational modes.[10] The classical case has been theoretically studied in the case of a single-level quantum dot,[11,12] as well as in the metallic case.[7,13–15]

Recent experiments[16,17] on suspended carbon nanotubes have observed a reduction of the mechanical resonance frequency of the fundamental bending mode at low-bias voltages and for V_g near the degenerate region. This effect is a precursor of the mechanical instability and, thus, of the current blockade. But the complete observation of the latter phenomenon is difficult since the typical value of E_E is only of a few μeV, thus, smaller than cryogenic temperatures. In order to increase E_E, one can increase the electrostatic coupling between the oscillator and the SET since E_E depends quadratically on F_e. But another way of strengthening the effect would be to reduce the spring constant k of the oscillator. The reason is that softer oscillators will displace more under the influence of the electrostatic force F_e, and, thus, will see a larger change in the gate voltage when electrons tunnel in. A way of reducing k in a controlled manner is to operate a doubly clamped beam subject to a lateral compression force F. The latter can bring the beam to the well-known Euler buckling instability[18,19] (see Fig. 1). Under the action of the force F, the system exhibits a continuous transition from a flat to a buckled state, while the fundamental bending mode becomes softer as one approaches the mechanical instability ($k \to 0$). It is clear that this does not imply a divergence of E_E, since, at the transition, anharmonic terms will modify the simple

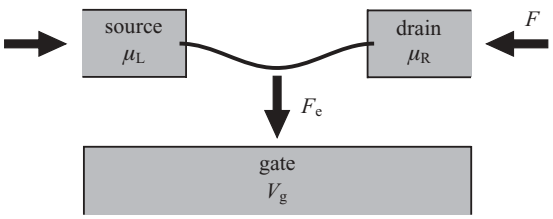

FIG. 1. Sketch of the considered system: a suspended doubly clamped beam forming a quantum dot electrically connected to source and drain electrodes held at chemical potentials μ_L and μ_R by the bias voltage V, respectively. The beam is capacitively coupled to a metallic gate kept at a voltage V_g, which induces a force F_e that attracts the beam toward the gate electrode. An additional externally controlled compressional force F acts on the beam and induces a buckling instability.

arguments given previously. However, a strong enhancement of E_E is expected. The Euler instability has been studied both experimentally[20–23] and theoretically[24–27] in micro- and nanomechanical systems. We have recently considered the Euler instability in NEMS for the case where F_e is negligible with respect to the intrinsic electron-phonon coupling.[28]

In this paper, we investigate, in detail, the idea of increasing the current blockade by exploiting the Euler instability, considering how the anharmonic terms, the temperature, and the nonequilibrium fluctuations modify the simplified picture given earlier. We find that, near the buckling instability, the current blockade induced by the mechanical resonator is strongly enhanced, rendering this effect experimentally observable.

The paper is structured as follows: In Sec. II, the model used to describe the system is introduced. In Sec. III, a statistical description in terms of a Fokker-Planck equation is given. Then, it is used in the remainder of the paper to determine the current and the mechanical behavior of the system. In Sec. IV, the enhancement of E_E is obtained at mean-field level. We discuss the effects of thermal and charge fluctuations on the results in Sec. V. In Sec. VI, we investigate the consequences of a finite average excess charge on the quantum dot for our results. Section VII presents some estimates of the effect we are predicting for recently realized experiments. We conclude in Sec. VIII. We relegate several technical issues to the appendices.

II. MODEL

As a representative model for the problem outlined in Sec. I, we consider a quantum dot embedded in a doubly clamped beam as shown in Fig. 1. The presence of the metallic gate near the dot is responsible for the coupling of the bending modes of the beam to the charge state of the dot. The Hamiltonian of the system can then be written as

$$H = H_{\rm vib} + H_{\rm SET} + H_{\rm c}, \tag{1}$$

where $H_{\rm vib}$ describes the oscillating modes of the nanobeam, $H_{\rm SET}$ takes into account the electronic degrees of freedom of the single-electron transistor, and $H_{\rm c}$ represents the coupling between the SET and the resonator. The model describes, for instance, transport through suspended carbon nanotubes as considered in the experiments of Refs. 10,16,17, and 29. Notice that the model also describes an alternative setup that may be realized experimentally, namely, a nonsuspended quantum dot coupled to a beamlike gate electrode to which a compressive strain is applied.

Using standard methods of elasticity theory, one can show that, close to the buckling instability, the frequency ω of the fundamental bending mode of the nanobeam vanishes, while those of the higher modes remain finite.[19] This allows one to retain only the fundamental mode parametrized by the displacement X of the center of the beam. As detailed in Appendix A, the Hamiltonian representing the oscillations of the nanobeam thus takes the Landau-Ginzburg form[21,24–26,28]

$$H_{\rm vib} = \frac{P^2}{2m} + \frac{m\omega^2}{2}X^2 + \frac{\alpha}{4}X^4, \tag{2}$$

where P is the momentum conjugate to X. For a doubly clamped uniform nanobeam of length L, linear mass density σ, and bending rigidity κ, one can show [25,26] that, close to the instability, the effective mass of the beam is $m = 3\sigma L/8$. The fundamental bending mode frequency reads

$$\omega = \omega_0\sqrt{1 - \frac{F}{F_{\rm c}}}, \tag{3}$$

where F is the compression force, $F_{\rm c} = \kappa(2\pi/L)^2$ is the critical force at which buckling occurs, and $\omega_0 = \sqrt{\kappa/\sigma}(2\pi/L)^2$. The positive parameter $\alpha = F_{\rm c}L(\pi/2L)^4$ ensures the stability of the system for $F > F_{\rm c}$.[30] For $F < F_{\rm c}$ ($\omega^2 > 0$), $X = 0$ is the only stable solution, and the beam remains straight. For $F > F_{\rm c}$, it buckles into one of the two metastable states at $X = \pm\sqrt{-m\omega^2/\alpha}$. Notice that, in writing Eq. (2), we assumed that the nanobeam cannot rotate around its axis due to clamping at its two ends.

Electronic transport is accounted for by the SET Hamiltonian consisting of three parts,

$$H_{\rm SET} = H_{\rm dot} + H_{\rm leads} + H_{\rm tun}, \tag{4}$$

where $H_{\rm dot}$ describes the quantum dot, $H_{\rm leads}$ describes the left (L) and right (R) leads, and $H_{\rm tun}$ represents the tunneling between leads and dot. Explicitly,

$$H_{\rm dot} = (\epsilon_{\rm d} - e\bar{V}_{\rm g})n_{\rm d} + \frac{U}{2}n_{\rm d}(n_{\rm d} - 1), \tag{5}$$

with $n_{\rm d} = d^\dagger d$, and $d^\dagger$ (d) creates (annihilates) an electron on the dot, $\bar{V}_{\rm g} = C_{\rm g}V_{\rm g}/C_\Sigma$, with $C_{\rm g}$ and C_Σ as the gate and total capacitances of the SET, respectively. The intradot Coulomb repulsion is denoted by U. In the following, we set $\epsilon_{\rm d} = 0$, measuring $V_{\rm g}$ from the degeneracy point. The left and right leads are assumed to be Fermi liquids at temperature T with chemical potentials $\mu_{\rm L}$ and $\mu_{\rm R}$ (measured from $\epsilon_{\rm d}$), respectively. A (symmetric) bias voltage V is applied to the junction such that $\mu_{\rm L} = -\mu_{\rm R} = eV/2$. The lead Hamiltonian reads

$$H_{\rm leads} = \sum_{ka}(\epsilon_k - \mu_a)\, c^\dagger_{ka}c_{ka}, \tag{6}$$

with c_{ka} as the annihilation operator for a spinless electron of momentum k in lead $a = {\rm L,R}$.[31] Finally, tunneling is accounted for by the Hamiltonian

$$H_{\rm tun} = \sum_{ka}(t_a c^\dagger_{ka}d + {\rm H.c.}), \tag{7}$$

with t_a as the tunneling amplitude between the quantum dot and the lead a.

Two different kinds of couplings exist between the electronic occupation of the dot $n_{\rm d}$ and the vibrational degrees of freedom: (i) An intrinsic one that originates from the variation of the electronic energy due to the elastic deformation of the beam,[32] and (ii) an electrostatic one, induced by the capacitive coupling to the gate electrode of the SET.[33–36] By symmetry, the former is quadratic in the amplitude X, and its effect on the Euler instability has been considered in Ref. 28. The latter is linear in X, and here we are interested in the case where the second coupling dominates over the first one. Their relative intensity is controlled by the distance h between

the gate electrode and the beam, since the intrinsic coupling does not depend on h, while the electrostatic force depends logarithmically on h.[33] Assuming that the beam is sufficiently close to the gate electrode such that the capacitive coupling dominates,[37] we can write

$$H_c = F_e X n_d, \tag{8}$$

where $-F_e$ is the force exerted on the tube when one excess electron occupies the quantum dot (see Fig. 1). The model assumes that the gate voltage is such that only charge states with $n_d = 0$ and 1 are accessible. For larger gate voltages overcoming the charging energy of the quantum dot, the charge on the dot will instead fluctuate between N and $N+1$. This induces an additional constant force bending the tube further. The effect of such a force on the classical current blockade will be discussed in Sec. VI. Notice that, in the case in which the suspended structure is the gate capacitance coupled to a static quantum dot, the intrinsic coupling is not present, and only the capacitive electromechanical coupling has to be taken into account.

III. FOKKER-PLANCK DESCRIPTION

We are interested in describing the vicinity of the instability where the relevant resonator frequency vanishes [see Eq. (3)]. The mechanical degree of freedom can then be treated classically since, for any reasonable temperature, $\hbar\omega \ll k_B T$. The softening of the mechanical mode also implies a natural separation of time scales between the slow mechanical mode and the fast electronic degrees of freedom, controlled by the typical tunneling rate Γ. Thus, as detailed in Appendix B, it is convenient to eliminate the fast modes and to obtain a Fokker-Planck equation for the probability distribution $\mathcal{P}(X,P,t)$ of the slow mode:[7,11,14,28,38]

$$\partial_t \mathcal{P} = -\frac{P}{m}\partial_X \mathcal{P} - F_{\rm eff}(X)\,\partial_P \mathcal{P} + \frac{\eta(X)+\eta_e}{m}\partial_P(P\mathcal{P}) + \left(\frac{D(X)}{2} + \eta_e k_B T\right)\partial_P^2 \mathcal{P}. \tag{9}$$

The effective force $F_{\rm eff}(X) = -\partial_X H_{\rm vib} + F_{\text{c-i}}(X)$ acting on the mechanical degree of freedom consists of two parts: a force arising from the Hamiltonian (2) of the nanobeam, $-\partial_X H_{\rm vib} = -m\omega^2 X - \alpha X^3$ and a current-induced conservative force $F_{\text{c-i}}(X) = -F_e n_0(X)$, proportional to the occupation of the dot averaged over a time long with respect to Γ^{-1}, but short with respect to the period of the mechanical motion, $n_0(X) = \langle n_d \rangle_X$. In Eq. (9), the diffusion constant $D(X)$ accounts for the fluctuations of the force associated with the coupling Hamiltonian (8) originating from the stochastic nature of the charge-transfer processes. Finally, retardation effects cause dissipation of the mechanical energy with damping coefficient $\eta(X)$.

To account for the quality factor $Q = m\omega_0/\eta_e$ of the nanobeam mode, the mechanical degree of freedom is coupled to an additional environment at equilibrium (such as, e.g., a generic phonon bath within the Caldeira-Leggett model[39]), implying dissipation and fluctuations controlled by an extrinsic damping constant η_e entering Eq. (9). This extrinsic damping comes from several mechanisms coupling the mechanical mode to other degrees of freedom: localized defects at the surface of the sample (thought to be the main source of dissipation in semiconductor resonators[40] and which can be modeled as two-level systems[41,42]), clamping losses, thermoelastic losses, Ohmic losses due to the gate electrode (which have been predicted to be the dominant source of extrinsic dissipation for graphene-based resonators in Ref. 43), etc. Due to the wide variety of these possible sources of extrinsic dissipation, we here assume, for simplicity, that they can all be lumped into the generic (Ohmic, memory-free[39]) damping constant η_e. Notice also that the phonon temperature of the bath is typically lower but of the same order as the electronic temperature T.[16] For simplicity, we assumed, in writing Eq. (9), that both temperatures coincide, as we do not expect a qualitative change of our results due to this assumption.

The explicit form of the coefficients entering into the Fokker-Planck equation (9) depends on the transport regime one considers (sequential or resonant transport), as well as on the nature of the quantum dot (metallic or single-level quantum dot). In this paper, we consider the case of a single level in the sequential tunneling regime, but a similar analysis can be carried out for the metallic (e.g., along the lines of Refs. 7,14,28) and the resonant transport regimes (cf. Refs. 11,12,38). To be specific, we assume that $\hbar\Gamma = \sum_{a=\text{L,R}} \hbar\Gamma_a \ll k_B T$ with $\Gamma_a = 2\pi|t_a|^2\nu/\hbar$ and ν as the density of states at the Fermi level of the leads. We also assume the intradot Coulomb repulsion $U \to \infty$ such that double occupancy of the dot is forbidden. In this transport regime, the position-dependent rates for tunneling into and out of the dot read[44]

$$\Gamma_{01}(X) = \sum_{a=\text{L,R}} \Gamma_a f_F\left(\frac{F_e X - e\bar{V}_g - \mu_a}{k_B T}\right), \tag{10}$$

$$\Gamma_{10}(X) = \sum_{a=\text{L,R}} \Gamma_a \left[1 - f_F\left(\frac{F_e X - e\bar{V}_g - \mu_a}{k_B T}\right)\right], \tag{11}$$

respectively, where $f_F(z) = (e^z+1)^{-1}$ is the Fermi function. Thus, the average occupation of the dot for a given mode amplitude X is

$$n_0(X) = \frac{\Gamma_{01}(X)}{\Gamma}, \tag{12}$$

and, as shown in Appendix B, we have $D(X) = 2F_e^2 n_0(X)[1 - n_0(X)]/\Gamma$ and $\eta(X) = -F_e\,\partial_X n_0(X)/\Gamma$ for the current-induced diffusion and damping terms in Eq. (9).[14,45] The average current I through the device can be obtained from the stationary solution of the Fokker-Planck equation (9), $\partial_t \mathcal{P}_{\rm st} = 0$, by averaging the position-dependent current

$$\mathcal{I}(X) = \frac{e\Gamma_L\Gamma_R}{\Gamma}\left[f_F\left(\frac{F_e X - e\bar{V}_g - eV/2}{k_B T}\right) - f_F\left(\frac{F_e X - e\bar{V}_g + eV/2}{k_B T}\right)\right] \tag{13}$$

with the phase-space distribution,

$$I = \int\!\!\int dX\,dP\,\mathcal{P}_{\rm st}(X,P)\mathcal{I}(X). \tag{14}$$

Before we proceed, it is convenient to introduce reduced variables in terms of the relevant energy scale of the

problem $E_{\rm E}^0 = F_{\rm e}^2/m\omega_0^2$, the polaronic shift $\ell = F_{\rm e}/m\omega_0^2$, and the vibrational frequency for vanishing compression force ω_0 [see Eq. (3)]. By denoting $x = X/\ell$, $p = P/m\omega_0\ell$, $\tau = \omega_0 t$, the Fokker-Planck equation (9) becomes

$$\partial_\tau \mathcal{P} = -p\,\partial_x \mathcal{P} - f_{\rm eff}(x)\,\partial_p \mathcal{P} + [\gamma(x) + \gamma_{\rm e}]\partial_p(p\mathcal{P}) + \left(\frac{d(x)}{2} + \gamma_{\rm e}\tilde{T}\right)\partial_p^2 \mathcal{P}, \tag{15}$$

with the scaled effective force given by

$$f_{\rm eff}(x) = \delta x - \tilde{\alpha}x^3 - n_0(x), \tag{16}$$

the reduced force $\delta = F/F_{\rm c} - 1$, and the anharmonicity parameter $\tilde{\alpha} = \alpha\ell^4/E_{\rm E}^0$. We further introduced a scaled current-induced diffusion constant

$$d(x) = \frac{2\omega_0}{\Gamma} n_0(x)[1 - n_0(x)], \tag{17}$$

and damping coefficient

$$\gamma(x) = -\frac{\omega_0}{\Gamma}\,\partial_x n_0\,(x). \tag{18}$$

In Eq. (15), $\gamma_{\rm e} = \eta_{\rm e}/m\omega_0 = Q^{-1}$, where Q is the quality factor of the mechanical resonator and $\tilde{T} = k_{\rm B}T/E_{\rm E}^0$. In these scaled units, the electromechanical coupling appears only in the coefficient of the quartic term, $\tilde{\alpha} = \alpha F_{\rm e}^2/(m\omega_0^2)^3$. It is important to notice that, for actual experiments on suspended carbon nanotubes,[16,17,29] $\tilde{\alpha} \ll 1$ as we will discuss more extensively in Sec. VII.

IV. MEAN-FIELD APPROACH: ENHANCEMENT OF THE CURRENT BLOCKADE

We begin our analysis by assuming $\omega_0/\Gamma \to 0$.[46] Note that the diffusion and dissipation coefficients $d(x)$ and $\gamma(x)$ in Eq. (15) are proportional to ω_0/Γ [cf. Eqs. (17) and (18)] so that this implies neglecting current-induced fluctuations. In this limit, the stationary solution for $\mathcal{P}$ is given by a Boltzmann distribution at temperature $\tilde{T}$,

$$\mathcal{P}_{\rm st}(x,p) = \mathcal{N}\,\exp\left(-\frac{p^2/2 + v_{\rm eff}(x)}{\tilde{T}}\right), \tag{19}$$

with $\mathcal{N}$ as a normalization constant. In order to obtain transparent analytical results, we also assume zero temperature (in fact, $\hbar\omega \ll k_{\rm B}T \ll E_{\rm E}^0$) such that the stationary probability distribution (19) becomes $\mathcal{P}_{\rm st}(x,p) = \delta(p)\delta(x - x_{\rm m})$. Here, $x_{\rm m}$ is the global minimum of the effective potential

$$v_{\rm eff}(x) = -\int^x dx'\, f_{\rm eff}(x') \tag{20}$$

corresponding to the effective force (16) and can be determined from the dynamical equilibrium equation

$$f_{\rm eff}(x) = 0, \quad \frac{df_{\rm eff}(x)}{dx} < 0. \tag{21}$$

Notice that the latter equation can have more than one solution such that the system is multistable. In this zero-temperature limit, the current can then easily be obtained from Eq. (14). Doing so, as a function of the gate and bias voltages, we can determine the Coulomb diamond for a given compression force δ. At zero temperature, one finds that there always exists a region at low-bias voltage where the current is suppressed.

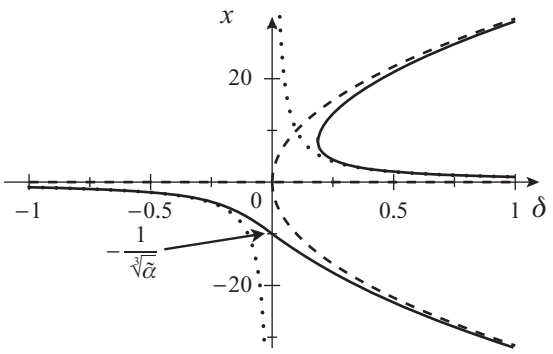

FIG. 2. Example of a solution $x(\delta)$ of the equation for dynamic equilibrium (21) for $n_0 = 0$ (dashed line), $n_0 = 1$ (solid line), and for $n_0 = 1$ and $\tilde{\alpha} = 0$ (dotted line). In the figure, $\tilde{\alpha} = 10^{-3}$.

To characterize this classical current blockade, we define Δ_v, the minimal value of bias voltage, for which a finite current flows through the device at zero temperature. It is useful to first derive a simple estimate of the maximally obtainable Δ_v. To do so, we solve the dynamic equilibrium equation (21) for $n_0 = 0$ and $n_0 = 1$, corresponding to empty and occupied central islands, respectively. For $n_0 = 0$, one has the solutions $x = 0$ for any δ and $x = \pm\sqrt{\delta/\alpha}$ for $\delta > 0$ of the pristine Euler instability (see Fig. 2, dashed line). For $n_0 = 1$, the solutions can easily be sketched for $\tilde{\alpha} \ll 1$ as an interpolation of the $\tilde{\alpha} = 0$ solutions (dotted line in Fig. 2) and the solutions for $n_0 = 0$. The exact result is shown as a solid line in Fig. 2. We are interested in the maximum shift in x that the system undergoes in response to a fluctuation of n_0 by one unit, Δx. It is apparent from the figure that this happens for $\delta = 0$ where $\Delta x = 1/\sqrt[3]{\tilde{\alpha}}$. The corresponding change in the effective potential (20) is $\Delta v_{\rm eff} \sim 1/\sqrt[3]{\tilde{\alpha}}$. This provides an estimate of the maximal energy gap generated by the electromechanical coupling and, thus, a good estimate of Δ_v. Notice that the previous simple argument is not specific to the transport model we are considering here, as the specific form of n_0 in the conducting region does not enter our argument. Thus, we expect that our estimate of a maximal gap $\Delta_v \sim 1/\sqrt[3]{\tilde{\alpha}}$ remains valid for metallic quantum dots as well as in the resonant transport regime.

We now turn to the complete solution of Eq. (21). For simplicity, we assume symmetric coupling to the leads ($\Gamma_{\rm L} = \Gamma_{\rm R} = \Gamma/2$) such that the average occupation of the dot at fixed x [entering into the effective force (16)] is obtained from the zero-temperature limit of Eqs. (10) and (12) and is given by

$$n_0(x) = \frac{1}{2}\left[\Theta\left(-x + v_{\rm g} + \frac{v}{2}\right) + \Theta\left(-x + v_{\rm g} - \frac{v}{2}\right)\right], \tag{22}$$

where $v = eV/E_{\rm E}^0$ (assumed positive for definiteness), $v_{\rm g} = e\bar{V}_{\rm g}/E_{\rm E}^0$, and $\Theta(z)$ is the Heaviside step function. In the most general case, we solve Eq. (21) numerically. However, transparent analytical expressions can be obtained in the limits $|\delta| \gg \sqrt[3]{\tilde{\alpha}}$ and $|\delta| \ll \sqrt[3]{\tilde{\alpha}}$. In particular, we can obtain explicit expressions for the value of v beyond which the current begins to flow, i.e., the gap Δ_v. To first order in the small parameter

$\sqrt[3]{\tilde{\alpha}}/|\delta|$ (far from the instability) and $|\delta|/\sqrt[3]{\tilde{\alpha}}$ (in the vicinity of the instability), we find that

$$\Delta_v = \begin{cases} -\dfrac{1}{2\delta}, & -1 \leqslant \delta \ll -\sqrt[3]{\tilde{\alpha}}, \\ \dfrac{1}{4\delta}, & \delta \gg \sqrt[3]{\tilde{\alpha}}, \\ \dfrac{\sqrt[3]{2}-1}{\sqrt[3]{\tilde{\alpha}}}\left(\dfrac{3}{2^{4/3}} - \dfrac{\delta}{\sqrt[3]{\tilde{\alpha}}}\right), & |\delta| \ll \sqrt[3]{\tilde{\alpha}}. \end{cases} \tag{23}$$

Far from the mechanical instability, the gap is simply given by the result of a harmonic theory (see Appendix C) where $\Delta_v = 1/2v''(\bar{x})$ with $v''(\bar{x})$ as the curvature of the bare potential $v(x)$ [i.e., the effective potential without the contribution from $n_0(x)$] at its global minimum $\bar{x}$. Far below the buckling instability ($-1 \leqslant \delta \ll -\sqrt[3]{\tilde{\alpha}}$), $\bar{x} = 0$ and $v''(\bar{x}) = -\delta$ such that $\Delta_v = -1/2\delta$. Far above the mechanical instability ($\delta \gg \sqrt[3]{\tilde{\alpha}}$), $\bar{x} = -\sqrt{\delta/\tilde{\alpha}}$ and $v''(\bar{x}) = 2\delta$ such that $\Delta_v = 1/4\delta$. As one approaches the buckling instability from below or above, the apparent divergences in the first two lines of Eq. (23) are cut off by the cubic term in x in the effective force (16), and for $|\delta| \ll \sqrt[3]{\tilde{\alpha}}$, the maximal gap $\Delta_v \sim 1/\sqrt[3]{\tilde{\alpha}}$ is reached.

The analytical results of Eq. (23) are compared to a numerical calculation of the gap in Fig. 3(a) for $\tilde{\alpha} = 10^{-3}$ and $\tilde{\alpha} = 10^{-6}$ (red dots and blue squares in the figure, respectively). It is evident from the figure that there is a dramatic increase of the gap close to the instability. Furthermore, the smaller $\tilde{\alpha}$, i.e., the smaller the electromechanical coupling, the larger is the increase of the gap at the instability relative to its value for vanishing compression force [see the inset in Fig. 3(a)]. However, of course, the maximal value of the gap in absolute terms increases with the strength of the electromechanical coupling as $F_e^{4/3}$. Thus, it would be of great experimental interest to exploit the Euler instability to obtain a clear signature of the classical current blockade in transport experiments on suspended quantum dots.

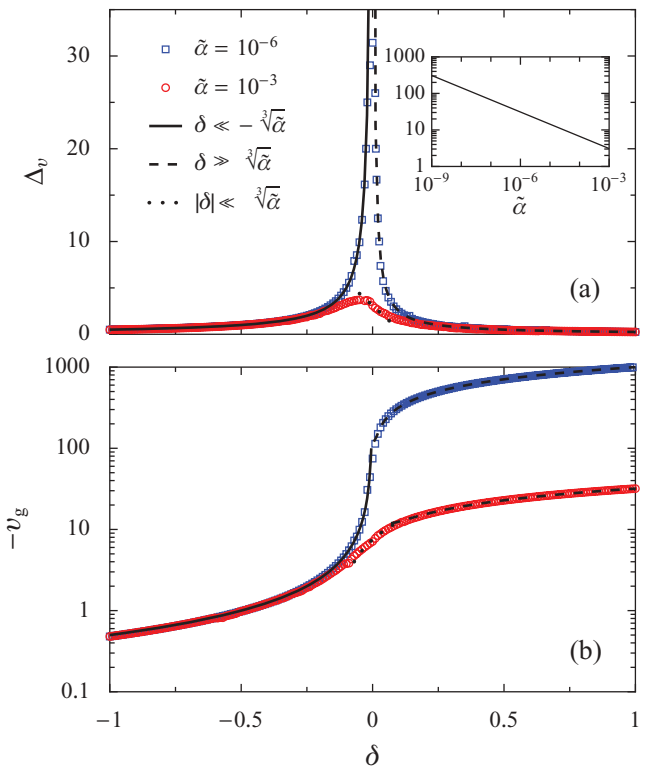

FIG. 3. (Color online) (a) Gap Δ_v and (b) gate voltage v_g (defined as the bias and gate voltages in reduced units at the apex of the Coulomb diamond, respectively) as a function of the scaled compression force $\delta = F/F_c - 1$. The red circles and blue squares are numerical results for $\tilde{\alpha} = 10^{-3}$ and 10^{-6}, respectively, which are compared to the asymptotic behaviors (23) and (24) for forces below (solid line), above (dashed line), and in the vicinity (dotted line) of the critical force F_c. (Inset) Gap $\Delta_v \sim 1/\sqrt[3]{\tilde{\alpha}}$ from Eq. (23) as a function of $\tilde{\alpha}$ at the mechanical instability ($\delta = 0$).

The gaps of Eq. (23) are obtained for values of the gate voltage approximately given by

$$v_g = \begin{cases} \dfrac{1}{2\delta}, & -1 \leqslant \delta \ll -\sqrt[3]{\tilde{\alpha}}, \\ -\dfrac{1}{4\delta} - \sqrt{\dfrac{\delta}{\tilde{\alpha}}}, & \delta \gg \sqrt[3]{\tilde{\alpha}}, \\ -\dfrac{1}{4\sqrt[3]{\tilde{\alpha}}}\left(3 + \dfrac{2\delta}{\sqrt[3]{\tilde{\alpha}}}\right), & |\delta| \ll \sqrt[3]{\tilde{\alpha}}, \end{cases} \tag{24}$$

which are shown in Fig. 3(b) and are compared to a numerical calculation. Equations (23) and (24) define the apexes of the Coulomb diamonds, which are shown in Fig. 4.

Thus, the effect of the compression force is to continuously displace the Coulomb diamond in the v-v_g plane toward negative gate voltages [see also Fig. 3(b)] and to open a gap, which is maximal close to the Euler instability at $\delta = 0$ [see Fig. 4(d)]. Note that the shift in gate voltage is strongly asymmetric about the Euler instability. While the shifts are only small below the Euler instability [see Figs. 4(a)–4(c) and Fig. 3(b)], the shifts in gate voltage are orders of magnitudes larger on the buckled side of the Euler instability [see Figs. 4(e)–4(g) and Fig. 3(b)]. In fact, it may be that these shifts would be the most easily detected consequence of the Euler buckling instability in NEMS. In Fig. 4, the bias and gate voltages are measured in units of the elastic energy E_E^0, which is of the order of a few μeV for typical experiments on suspended carbon nanotubes (see Sec. VII). The smallness of this energy scale explains why the scaled numerical values of the shifts become so large on the buckled side of the Euler instability.

It is also interesting to comment on the shape of the Coulomb blockade diamond. In Ref. 28, we showed, for the case of intrinsic electron-phonon coupling (quadratic in x) and for a metallic quantum dot, that the Euler buckling instability leads to nonlinear deformations of the Coulomb diamonds, a phenomenon that we have named tricritical current blockade. In contrast, our present results show that, for a capacitive electromechanical coupling (linear in x) and for a single-level quantum dot, the shape of the Coulomb diamond remains unchanged. The conventional triangular shape in the v-v_g plane is delineated by straight lines with $v \sim \pm 2v_g$ for any value of the compressive strain. As we have checked,[47] the difference between the present results and those of Ref. 28 is due to the difference in the transport models considered (metallic vs single-level quantum dot) and not to the type of electromechanical coupling (intrinsic vs extrinsic). Specifically, we find that the difference is due to

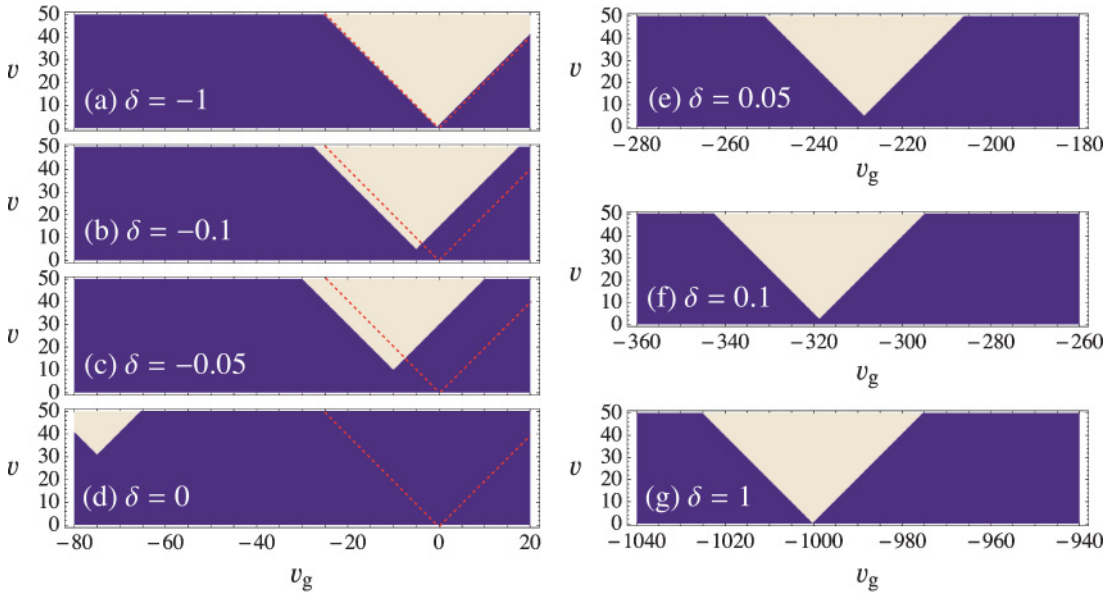

FIG. 4. (Color online) Mean-field current I at zero temperature and for symmetric coupling to the leads ($\Gamma_L = \Gamma_R = \Gamma/2$) as a function of bias v and gate voltage v_g (measured in units of the elastic energy E_E^0). The (scaled) compression force δ increases from (a) to (g). Notice that the scale of the v_g axis is different in (e), (f), and (g) and in (a)–(d). The red dashed lines indicate the position of the Coulomb diamond in the absence of electromechanical coupling ($F_e = 0$). In the figure, $\tilde{\alpha} = 10^{-6}$, and dark blue and white regions correspond to $I = 0$ and $I = e\Gamma/4$, respectively.

the fact that, in the single-level case, the average occupation of the dot abruptly jumps as a function of gate voltage, while in the metallic case, this occupation gradually changes due to the continuous density of states of the dot. Notice also that, for intrinsic electromechanical coupling, the Coulomb diamond is not influenced by the latter for compression forces below the critical force ($\delta < 0$), in contrast to the present case. This is due to the fact that, in the flat state, the quadratic electromechanical coupling merely represents a renormalization of the fundamental bending mode frequency and does not lead to current blockade.

It is instructive to make the analogies with standard results of Landau mean-field theory for continuous phase transitions[48] explicit. According to Eq. (21) governing the dynamical equilibrium, we can make the following identifications: x corresponds to the order parameter in Landau theory, δ corresponds to the reduced temperature, and $\tilde{\alpha}$ corresponds to the coefficient of the quartic term in the Landau free energy. Finally, n_0 plays a role similar to a symmetry-breaking (magnetic) field. In the present case, this field is, in general, dependent on x, which has no correspondence in Landau theory. Nevertheless, the analogy between n_0 and a magnetic field is helpful since some of our results can be understood by comparing the situations with zero ($n_0 = 0$) and one ($n_0 = 1$) electrons on the dot, as illustrated by the foregoing estimate for the maximal Δ_v (see Fig. 2).

With these correspondences, we can now establish analogies between some of our results and standard results of Landau theory. To start with, the dependence of the displacement $x \sim \pm\delta^{1/2}$ in the buckled state is analogous to the result of Landau theory that the order parameter exponent is $\beta = 1/2$. Given that Δ_v depends linearly on x, we can also interpret the relations in Eq. (23) in terms of Landau theory. Let us start with the case of small δ in the immediate vicinity of the instability. In this case, we find that $\Delta_v \sim \tilde{\alpha}^{-1/3}$. The exponent of $\tilde{\alpha}$ corresponds to the critical exponent $\delta = 3$ of Landau theory governing the dependence of the order parameter on the symmetry-breaking field at the critical temperature. Further from the instability, we have $\Delta_v \sim 1/|\delta|$. This relation is related to the familiar Curie law for the order parameter (or the susceptibility) as a function of temperature in an external field with mean-field critical exponent $\gamma = 1$.

Let us finally emphasize that the analogy with Landau theory is restricted to the mean-field level, since contrary to critical phenomena where an infinite number of modes is present, the system we describe is constituted by a single mode. Moreover, beyond mean-field theory, fluctuations in Landau theory are purely thermal, while in the present context, nonequilibrium fluctuations play an essential role. It is the effects of these fluctuations, which we turn to in Sec. V.

V. THERMAL AND CURRENT-INDUCED FLUCTUATIONS

We now go beyond the mean-field results of Sec. IV by taking into account the effects of the thermal as well as the current-induced fluctuations. It is physically clear that these fluctuations will lead to a smoothening of the current blockade at low-bias voltages as the system can explore more conducting states in phase space.

A. Temperature effects

We first neglect the current-induced fluctuations and focus on thermal fluctuations only. As discussed in Sec. IV, this becomes asymptotically exact in the extreme adiabatic limit of $\omega_0/\Gamma \to 0$, where the terms $\gamma(x)$ and $d(x)$ can be dropped from Eq. (15). The stationary solution for $\mathcal{P}$ is then given by

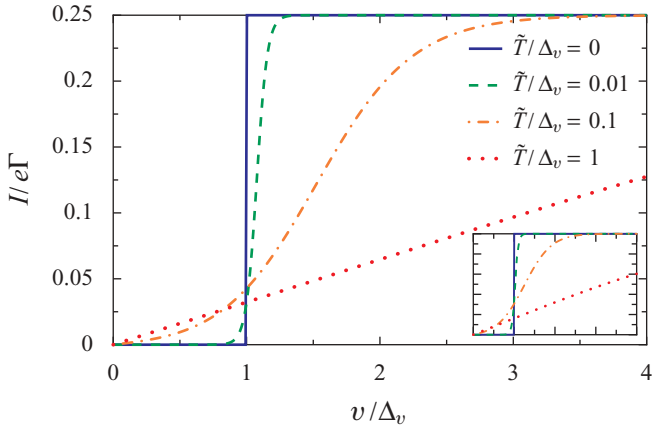

FIG. 5. (Color online) Current I at the apex of the Coulomb diamond as a function of bias v scaled by the energy gap Δ_v for various values of $\tilde{T}/\Delta_v$ and for compression forces in the vicinity of the buckling instability ($|\delta| \ll \sqrt[3]{\tilde{\alpha}}$). In the figure, only the temperature-induced fluctuations are considered. (Inset) Same as the main figure for compression forces far from the buckling instability ($|\delta| \gg \sqrt[3]{\tilde{\alpha}}$).

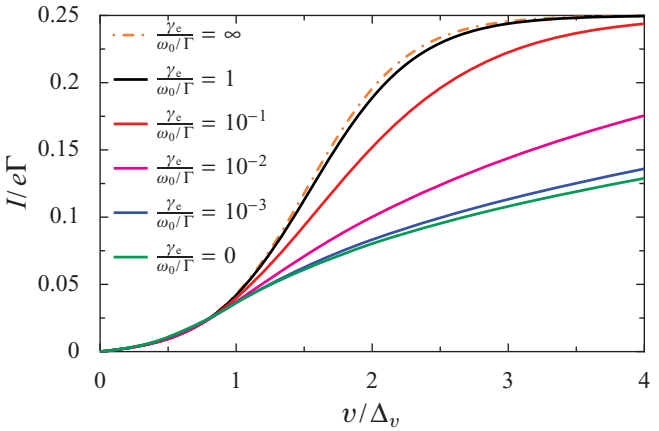

FIG. 6. (Color online) Current I at the apex of the Coulomb diamond for $\delta = 0$ as a function of v/Δ_v for $\tilde{\alpha} = 10^{-6}$ and $\tilde{T}/\Delta_v = 0.1$. (Solid lines) Nonequilibrium Langevin dynamics for $\frac{\gamma_e}{\omega_0/\Gamma} = 1, 10^{-1}$, 10^{-2}, 10^{-3}, and 0, from the highest to the lowest curve at large bias. (Dashed-dotted line) Fully adiabatic limit ($\frac{\gamma_e}{\omega_0/\Gamma} = \infty$), i.e., current only including thermal fluctuations (cf. dashed-dotted curve in Fig. 5). In our numerical calculations, we used $\omega_0/\Gamma = 10^{-2}$.

the Boltzmann distribution (19) with the effective potential

$$v_{\rm eff}(x) = -\frac{\delta x^2}{2} + \frac{\tilde{\alpha}x^4}{4} + x + \frac{\tilde{T}}{2}\ln\left[f_{\rm F}\left(\frac{x - v_{\rm g} + v/2}{\tilde{T}}\right)\right] + \frac{\tilde{T}}{2}\ln\left[f_{\rm F}\left(\frac{x - v_{\rm g} - v/2}{\tilde{T}}\right)\right]. \quad (25)$$

The current can now be calculated easily by numerical integration of Eq. (14) with Eq. (19). The result is shown in Fig. 5 as a function of the bias voltage for gate voltages corresponding to the apex of the modified zero-temperature Coulomb diamond [cf. Eq. (24)]. Once plotted as a function of v/Δ_v, one finds that the current behavior is similar at the transition (Fig. 5) and far from the transition (inset of Fig. 5). In both cases, the low-bias blockade of the current becomes less pronounced as temperature increases and vanishes completely for temperatures of the order of the gap Δ_v. As shown in Appendix D [cf. Eq. (D1)], the current has a Fermi-function-like behavior as a function of the bias voltage for temperatures much smaller than the energy gap Δ_v (see dashed and dashed-dotted lines in Fig. 5). Thus, it is exponentially suppressed for bias voltage below the gap. At larger temperatures, Eq. (D4) shows that the current is linear in the bias voltage (see dotted line in Fig. 5).

Our numerical and analytical results (cf. Appendix D) thus confirm that tuning the system near the buckling instability where Δ_v dramatically increases allows one to enlarge the temperature region over which the current blockade is observable.

B. Nonequilibrium dynamics close to the mechanical instability

We now consider the nonequilibrium Langevin dynamics of the nanobeam by solving the full Fokker-Planck equation (15). This is done by discretization of the Fokker-Planck equation and solution of the resulting linear system. We focus on the transition region ($\delta = 0$) and calculate the current for $v_{\rm g}$ at the apex of the Coulomb diamond [see Eq. (24) and Fig. 3(b)] and temperature lower than the gap $\tilde{T}/\Delta_v = 0.1$. Before we present our results, we notice that, for $(\omega_0/\Gamma, \gamma_e) \ll 1$, we can show that the stationary distribution of the Fokker-Planck equation approximately only depends on the ratio $\frac{\gamma_e}{\omega_0/\Gamma}$, a result we have also checked numerically (see Appendix E for details). The reason for this behavior is that, for $(\omega_0/\Gamma, \gamma_e) \ll 1$, the stationary distribution is almost a function of the (reduced) energy $E = p^2/2 + v_{\rm eff}(x)$ only.

Numerical results for the current are shown in Fig. 6 for various ratios of the inverse quality factor $Q^{-1} = \gamma_e$ as quantified by the damping coefficient γ_e and the adiabaticity parameter ω_0/Γ. Our principal observation is that the current blockade becomes sharper for low-Q resonators.

One can qualitatively understand the behavior of the current in Fig. 6 by defining an effective temperature of the system,

$$\tilde{T}_{\rm eff} = \frac{\langle d\rangle/2 + \gamma_e\tilde{T}}{\langle\gamma\rangle + \gamma_e}, \quad (26)$$

in close analogy with the fluctuation-dissipation theorem.[49] In Eq. (26), $\langle d\rangle$ and $\langle\gamma\rangle$ are the averages over the phase-space probability distribution of the current-induced fluctuations and dissipation [cf. Eqs. (17) and (18)], respectively. Notice that the strength of these two quantities is controlled by the adiabaticity parameter ω_0/Γ.

As one can see from Fig. 6, for $v < \Delta_v$, the current is almost insensitive to the quality factor and is the same as without current-induced fluctuations (see dashed-dotted line in Figs. 5 and 6). Using Eqs. (17) and (18), we have

$$d(x) = 2\gamma(x)\tilde{T} + \frac{\omega_0}{2\Gamma}\left[f_{\rm F}\left(\frac{x - v_{\rm g} - v/2}{\tilde{T}}\right) - f_{\rm F}\left(\frac{x - v_{\rm g} + v/2}{\tilde{T}}\right)\right]^2 \quad (27)$$

for symmetric coupling to the leads. However, for $v < \Delta_v$, positions x for which the current $\mathcal{I}(x)$ of Eq. (13) is suppressed are most stable (see dashed line in Fig. 7) such

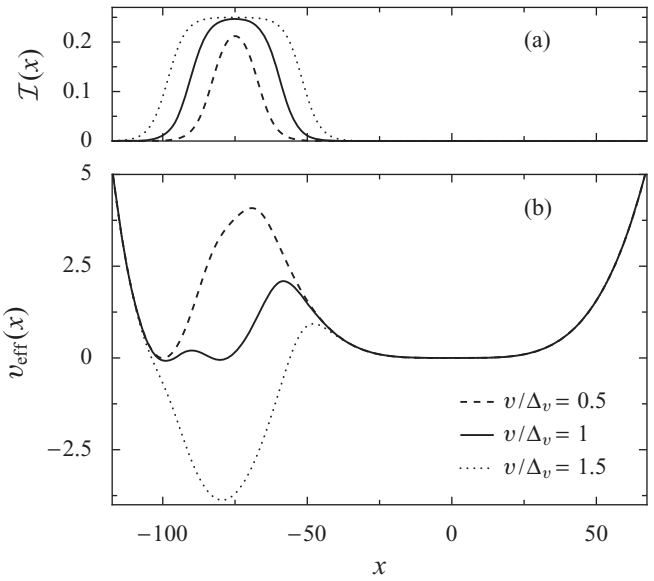

FIG. 7. (a) Current $\mathcal{I}$ as a function of x [Eq. (13)] and (b) effective potential $v_{\rm eff}(x)$ [Eq. (25)] for bias voltages below (dashed line), above (dotted line), and at (solid line) the energy gap Δ_v. The parameters are the same as in Fig. 6, i.e., $\delta = 0$, $\tilde{\alpha} = 10^{-6}$, $\tilde{T}/\Delta_v = 0.1$, and $v_{\rm g} = -3/4\sqrt[3]{\tilde{\alpha}}$.

that the current-induced diffusion and damping constants approximately satisfy a local fluctuation-dissipation theorem for all relevant positions x that are significantly populated, $d(x) \simeq 2\tilde{T}\gamma(x)$. We thus have $\langle d\rangle \simeq 2\tilde{T}\langle\gamma\rangle$, and according to the definition (26), we have $\tilde{T}_{\rm eff} \simeq \tilde{T}$. Hence, for bias voltages lower than the energy gap Δ_v, the current-induced fluctuations behave as the thermal ones, essentially keeping the mechanical system at equilibrium.

On the contrary, for $v > \Delta_v$, positions x, for which the system is conducting, are the most stable ones (see dotted line in Fig. 7), and one has $\langle d\rangle \simeq \omega_0/2\Gamma$, while $\langle\gamma\rangle$ is exponentially small. The mechanical system is then subject to strong nonequilibrium fluctuations. For $\langle\gamma\rangle \ll \gamma_{\rm e}$, we thus have, from Eq. (26), $\tilde{T}_{\rm eff} \simeq \tilde{T} + \frac{\omega_0/\Gamma}{4\gamma_{\rm e}}$. This estimate of the effective temperature shows that the system becomes hotter as the ratio $\frac{\gamma_{\rm e}}{\omega_0/\Gamma}$ decreases.[50] Hence, the system can explore more states in phase space for which $\mathcal{I}(x)$ is suppressed, and, in turn, the current decreases for decreasing $\frac{\gamma_{\rm e}}{\omega_0/\Gamma}$ for $v > \Delta_v$ (see Fig. 6). The latter argument breaks down when $\gamma_{\rm e} \ll \langle\gamma\rangle$. In that case, we can estimate the effective temperature self-consistently, by assuming that the phase-space distribution is a Boltzmann distribution at the temperature $\tilde{T}_{\rm eff}$. Approximating the effective potential by its zero-temperature expression and averaging $d(x)$ and $\gamma(x)$ over the effective Boltzmann distribution, we find for $v \gg \Delta_v$

$$\tilde{T}_{\rm eff} = \frac{\pi\Delta_v}{128A}\exp\left(\frac{Av^2}{\Delta_v\tilde{T}_{\rm eff}}\right), \tag{28}$$

with $A = 9(1-2^{-1/3})/2^{11/3}$. We thus have $\tilde{T}_{\rm eff}/\Delta_v \sim (v/\Delta_v)^2/\ln(v/\Delta_v) \gg \tilde{T}/\Delta_v$, which explains why, for $\gamma_{\rm e} = 0$, the current is more suppressed than for finite $\gamma_{\rm e}$. It is also interesting to note that this estimate of the effective temperature is much larger than for a metallic quantum dot, where $\tilde{T}_{\rm eff} \sim v$ (Ref. 13). The reason for this difference is that, in the metallic case, the fluctuation and the dissipation are of the same order inside the bias window, while in the single-level case, the average dissipation is exponentially suppressed as $\gamma(x)$ only has a significant contribution for positions x corresponding to the borders of the Coulomb diamond [see Eq. (18)].

Our results show that a low-quality factor is more suitable for the observation of the current blockade in classical resonators. It is interesting to note that this conclusion is also valid in the quantum case,[8,9] where the Franck-Condon blockade is more pronounced for fast equilibration of the vibron mode. Due to the scaling of our results for the classical current blockade with the parameter $\frac{\gamma_{\rm e}}{\omega_0/\Gamma}$ (see Fig. 6), we also conclude that it is advantageous for the observation of this phenomenon to have a resonator, which is slow compared to the tunneling dynamics, i.e., $\omega_0 \ll \Gamma$.

VI. EFFECT OF A FINITE EXCESS CHARGE ON THE QUANTUM DOT

Within the transport model of a single resonant electronic level with infinite charging energy that we have used so far, the number of electrons on the dot can only vary between 0 and 1 (see Sec. II). More generally, the range of gate voltages can exceed the charging energy, and the average number of excess electrons N on the dot can be much larger than 1. Due to these excess electrons, an additional force $-F_N$ further bends the nanotube and hence, increases its vibrational frequency.[16,17] Thus, we can expect that the bias voltage below which the current is blocked will decrease when N increases.

In order to investigate the effect of a nonvanishing average excess charge on the quantum dot, we assume that the gate voltage is such that there is either N or $N+1$ electrons on the dot. We measure the fluctuation of the dot occupation $n_{\rm d}$ with respect to N and incorporate the resulting additional force in Eq. (16) by writing $f_{\rm eff}(x) = \delta x - \tilde{\alpha}x^3 - n_0(x) - f_N$, where $f_N = F_N/F_{\rm e}$. We neglect thermal and current-induced fluctuations and work within a mean-field approximation at zero temperature such that $n_0(x)$ is given by Eq. (22). For finite f_N, the bare potential $v(x)$ (i.e., without the current-induced contribution) can be approximated by a harmonic potential close to its global minimum $\bar{x}$ such that the bias voltage below which the current is blocked is given by $\Delta_v = 1/2v''(\bar{x})$ (see Appendix C). The energy gap (resulting from the most stable solution of $\delta\bar{x} - \tilde{\alpha}\bar{x}^3 = f_N$) is plotted in Fig. 8(a), and the gate voltage at the apex of the Coulomb diamond is plotted in Fig. 8(b). As anticipated, the increase of the energy gap close to the mechanical instability is reduced as f_N increases. Moreover, the displacement of the Coulomb diamond in $v_{\rm g}$ is less pronounced for large f_N.

Far from ($|\delta| \gg \sqrt[3]{\tilde{\alpha}f_N^2}$) and in the vicinity of ($|\delta| \ll \sqrt[3]{\tilde{\alpha}f_N^2}$) the Euler instability, we analytically find for the gap

$$\Delta_v = \begin{cases} -\dfrac{1}{2\delta}, & -1 \leqslant \delta \ll -\sqrt[3]{\tilde{\alpha}f_N^2}, \\ \dfrac{1}{4\delta}, & \delta \gg \sqrt[3]{\tilde{\alpha}f_N^2}, \\ \dfrac{1}{6\sqrt[3]{\tilde{\alpha}f_N^2}}\left(1 - \dfrac{\delta}{3\sqrt[3]{\tilde{\alpha}f_N^2}}\right), & |\delta| \ll \sqrt[3]{\tilde{\alpha}f_N^2}, \end{cases} \tag{29}$$

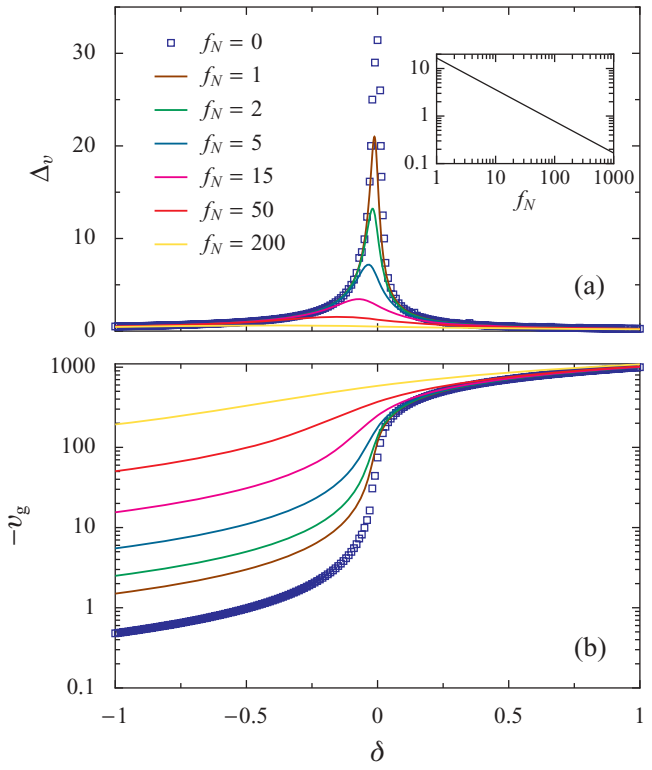

FIG. 8. (Color online) (a) Gap Δ_v and (b) gate voltage v_g at the apex of the Coulomb diamond for $\tilde{\alpha} = 10^{-6}$ as a function of the scaled compression force δ for increasing values of f_N [from top to bottom and bottom to top at $\delta = 0$ in (a) and (b), respectively]. The blue squares ($f_N = 0$) correspond to the numerical results of Fig. 3, while the solid lines result from the harmonic approximation (see text). (Inset) Gap $\Delta_v \sim 1/f_N^{2/3}$ from Eq. (29) as a function of f_N at the mechanical instability ($\delta = 0$).

to first order in the small parameter $\sqrt[3]{\tilde{\alpha} f_N^2}/|\delta|$ (far from the instability) and $|\delta|/\sqrt[3]{\tilde{\alpha} f_N^2}$ (in the vicinity of the instability). Far below and above the instability, the gap follows the same behavior as for $f_N = 0$ [see Eq. (23)]. This is due to the fact that, for large $|\delta| \gg f_N$, the stable position of the beam is similar to the one for $f_N = 0$. In the vicinity of the instability, the gap is reduced as f_N increases as $1/f_N^{2/3}$ (see the inset in Fig. 8). The reduction of the maximal gap close to the instability is a direct consequence of the smoothening of the mechanical transition between flat and buckled states due to the presence of the symmetry-breaking force f_N, similar to the behavior of the order parameter at a second-order phase transition in a symmetry-breaking field.[48]

We can estimate the force above which the increase of the gap at the instability completely vanishes by equating, in Eq. (29), the gap at, say, $\delta = -1$ and $\delta = 0$. We obtain that the increase of the gap should vanish once $f_N \gtrsim 1/\sqrt{3^3\tilde{\alpha}}$. Since for large N, $F_N \simeq F_e N/2$, this means that, if the average charge on the dot $N \gtrsim 2/\sqrt{3^3\tilde{\alpha}}$, the increase of the gap at the instability completely disappears. Since $\tilde{\alpha}$ is typically small (see Sec. VII), we expect that a significant increase of the current blockade at the mechanical instability persists for a wide range of gate voltages.

VII. EXPERIMENTAL REALIZATION

The electromechanical coupling (8) is typically weak in experiment. For this reason, only a precursor of the classical current blockade has been seen in two recent experiments on suspended carbon nanotube quantum dots,[16,17] but the full current blockade has not yet been observed. Indeed, we can obtain an estimate for the frequency shift of the fundamental bending mode, induced by the electromechanical coupling, from the effective potential associated with $F_{\rm eff}(X)$. The shift arises from the position dependence of $n_0(X)$. Expanding the current-induced force for weak electromechanical coupling, we find

$$F_{\text{c-i}}(X) \simeq -F_e n_0(0) - F_e^2 \left.\frac{\partial n_0}{\partial e\bar{V}_g}\right|_{F_e=0} X, \tag{30}$$

i.e., the current-induced force generates a term in the effective potential, which is quadratic in X. Far from the current-induced instability, this term gives a small renormalization of the resonance frequency, $\Delta\omega_0/\omega_0 = (E_E^0/2)\ \partial n_0/\partial e\bar{V}_g\big|_{F_e=0}$, from which we can extract a reliable estimate of the energy scale of the current blockade,

$$E_E^0 = \frac{2C_g}{C_\Sigma}\frac{\Delta\omega_0}{\omega_0}\left(\left.\frac{\partial n_0}{\partial e V_g}\right|_{F_e=0}\right)^{-1}. \tag{31}$$

From the experiments of Refs. 16 and 17, we extract a value of $\Delta\omega_0/\omega_0$ of a few percents for V_g at the degeneracy point. The derivative of n_0 with respect to $e\bar{V}_g$ can be estimated as the inverse of the width of the conductance peak in the V-V_g plane, divided by C_g/C_Σ. This last quantity can, in turn, be estimated from the slope of the Coulomb diamonds. Collecting these ingredients, we find that, for the suspended carbon nanotubes of Ref. 16, $E_E^0 \simeq 3$–$5\ \mu$eV, which corresponds to $\tilde{\alpha} \simeq 10^{-10}$, while for those of Ref. 17, we get $E_E^0 \simeq 20\ \mu$eV and $\tilde{\alpha} \simeq 10^{-8}$ (see Ref. 30).

We now use these numbers to estimate the possible enhancement of the current blockade near the Euler buckling instability. Based on Eq. (23), these parameters yield a possible increase of the mechanically induced gap by 3 orders of magnitude, leading to a maximal Δ_v (converted into a dimensionful quantity using the energy scale E_E^0) of the order of 3–5 meV. Such large gaps would be much more easily observable in experiment. The implementation of such a device could be performed by the method routinely employed to control break junctions through a force pushing the substrate of the device.

We also emphasize here again that it is preferable to operate the system near zero excess charge on the quantum dot where there are only a few electrons on the nanotube such that the increase of the energy gap close to the Euler instability is not smeared out by the additional force exerted on the nanotube (see Sec. VI). However, for the parameters of Refs. 16 and 17, we estimate that the enhancement of the current blockade remains very substantial for any realistic value of the excess charge.

When the tunneling-induced width Γ becomes larger than or of the order of temperature, cotunneling effects tend to smear the current blockade,[9,12] as direct electronic transitions between left and right leads take place. However, close to

the buckling instability, the gap may remain larger than the temperature so that cotunneling corrections should be suppressed in the immediate vicinity of the instability.

A last comment is in order on the required precision in the control of the lateral compression force F. As mentioned before, the increase of Δ_v is larger for smaller $\tilde{\alpha}$. But at the same time, the increase is limited to a small force range. The increase of the gap near the transition goes as $1/|F - F_c|$. Thus, when $\tilde{\alpha}$ is very small, a stringent requirement will be the precision in F that we denote by δF. In this case, the maximal gap will be of the order of $\frac{3}{4\pi}\frac{F_c}{\delta F}\ln(\frac{\delta F/F_c}{\sqrt[3]{\tilde{\alpha}}})$, assuming that $\delta F/F_c \gg \sqrt[3]{\tilde{\alpha}}$. This result can easily be checked by convolution of the gap (23) with a Lorentzian of width δF. This implies that, if one is able to control the force with a precision sufficient to see the buckling instability ($\delta F/F_c \ll 1$), there remains a large enhancement of the gap.

VIII. CONCLUSIONS

In this paper, we have investigated the consequences of a capacitive electromechanical coupling in a suspended single-electron transistor when the supporting beam is brought close to the Euler buckling instability by a lateral compression force. Our main result is that the low-bias current blockade originating from the coupling between the electronic degrees of freedom and the classical resonator can be enhanced by several orders of magnitude in the vicinity of the instability. We show that both the mechanical as well as the electronic properties of this regime can be described in an asymptotically exact manner based on a Langevin equation. These results are a direct consequence of the continuous nature of the Euler buckling instability and the associated critical slowing down of the fundamental bending mode of the beam at the instability. In fact, more generally, our results frequently have close and instructive analogies with the mean-field theory of second-order phase transitions. We focused on the sequential-tunneling transport regime of single-level quantum dots, but many of our qualitative results should remain valid also in the metallic case as well as for the resonant transport regime.[47] In fact, our basic approach should apply quite generally for any *continuous* mechanical instability of a nanoelectromechanical system.

Our results apply most directly to quantum dots situated on nanobeams or carbon nanotubes. Applying strain to the nanobeam in a controlled manner could, in principle, be experimentally performed with the help of a break junction. In fact, it is quite conceivable that, e.g., some carbon nanotube structures happen to be close to the Euler instability due to specifics in the fabrication of individual nanostructures. Our predictions may be helpful to identify such anomalous (and potentially interesting) samples.

ACKNOWLEDGMENTS

We acknowledge stimulating discussions with Eros Mariani, as well as financial support by Agence Nationale de la Recherche Contract No. JCJC-036 NEMESIS, and by the Deutsche Forschungsgemeinschaft through Sonderforschungsbereiche 658.

APPENDIX A: ELASTICITY THEORY OF THE EULER INSTABILITY

The elastic Lagrangian of a homogeneous rod of constant length L fixed at its two ends consists of three parts,

$$\mathcal{L} = \mathcal{T} - \mathcal{V}_b - \mathcal{V}_F. \tag{A1}$$

The kinetic term reads

$$\mathcal{T} = \frac{\sigma}{2}\int_0^L ds\, \dot{h}^2, \tag{A2}$$

where σ is the linear mass density, s is the arc length along the rod, and $h(s,t)$ is the displacement of the rod with respect to the u axis (see Fig. 9). The bending energy, controlled by the bending rigidity κ, is given by

$$\mathcal{V}_b = \frac{\kappa}{2}\int_0^L ds \left|\frac{d\hat{t}}{ds}\right|^2 = \frac{\kappa}{2}\int_0^L ds\, \frac{h''^2}{1-h'^2}, \tag{A3}$$

where $\hat{t} = (u',h')$ is the tangent vector of the rod and primes denote derivatives with respect to s. The last term in Eq. (A1) corresponds to the work done by the compression force F on the rod and reads

$$\mathcal{V}_F = -F(L - u_{\max}) = -F\int_0^L ds\left(1 - \sqrt{1-h'^2}\right), \tag{A4}$$

where $u_{\max}$ is the total extent of the rod along the u axis (see Fig. 9).

For small deflections ($|h'| \ll 1$), the Lagrangian (A1) becomes, in harmonic approximation,

$$\mathcal{L} \simeq \int_0^L ds\left(\frac{\sigma}{2}\dot{h}^2 - \frac{\kappa}{2}h''^2 + \frac{F}{2}h'^2\right), \tag{A5}$$

with the corresponding Euler-Lagrange equation

$$\sigma\ddot{h} + \kappa h'''' + Fh'' = 0. \tag{A6}$$

Equation (A6) can be solved by the eigenfunctions $h(s,t) = \sum_n h_n(s,t) = \sum_n X_n(t)g_n(s)$, where $g_n(s)$ are the normal modes, which follow from the solution of the characteristic equation. The frequency of the mode n reads

$$\omega_n^2 = \frac{\kappa}{\sigma}q_n^2\left(q_n^2 - \frac{F}{\kappa}\right), \tag{A7}$$

with q_n as the associated wave number, which depends on the considered boundary conditions. The vibrational frequency of the fundamental bending mode ($n = 1$) thus vanishes at the critical force $F_c = \kappa q_1^2$, while all higher modes have a finite frequency and, hence, are neglected in what follows. For $F > F_c$, the fundamental mode is unstable, and quartic corrections to the Lagrangian are necessary to ensure global stability.

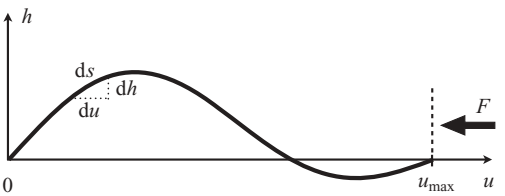

FIG. 9. Coordinate system used to describe the elastic properties of the rod.

TABLE I. Parameters entering the effective Lagrangian (A8) and the vibrational Hamiltonian (2).

Boundary conditions	$g_1(s)$	F_c	ω^2	m	α
$h\|_{0,L} = h''\|_{0,L} = 0$	$\sin\left(\frac{\pi s}{L}\right)$	$\kappa\left(\frac{\pi}{L}\right)^2$	$\frac{\kappa}{\sigma}\left(\frac{\pi}{L}\right)^4\left(1-\frac{F}{F_c}\right)$	$\frac{\sigma L}{2}$	$F_c L\left(\frac{\pi}{2L}\right)^4$
$h\|_{0,L} = h'\|_{0,L} = 0$	$\approx\sin^2\left(\frac{\pi s}{L}\right)$	$\kappa\left(\frac{2\pi}{L}\right)^2$	$\frac{\kappa}{\sigma}\left(\frac{2\pi}{L}\right)^4\left(1-\frac{F}{F_c}\right)$	$\frac{3\sigma L}{8}$	$F_c L\left(\frac{\pi}{2L}\right)^4$

Denoting $\omega_1 = \omega$ and $X_1 = X$, expanding the Lagrangian (A1) to quartic order in the displacement and inserting the solution h_1 of the harmonic problem, we thus obtain the effective Lagrangian close to the Euler instability,

$$\mathcal{L} = \frac{m}{2}\dot{X}^2 - \frac{m\omega^2}{2}X^2 - \frac{\alpha}{4}X^4, \tag{A8}$$

with the effective mass

$$m = \sigma\int_0^L ds\, g_1^2, \tag{A9}$$

and

$$\alpha = \int_0^L ds\left(2\kappa g_1''^2 g_1'^2 - \frac{F_c}{2}g_1'^4\right), \tag{A10}$$

with $g_1(L/2) = 1$ such that X corresponds in Eq. (A8) to the actual displacement of the center of the rod. Notice that *a priori*, α depends on the force F. However, close to the buckling instability, we can approximate $F \simeq F_c$ in Eq. (A10).

The parameters entering the effective Lagrangian (A8) and the corresponding vibrational Hamiltonian (2) are given in Table I for two types of boundary conditions: hinged end points ($h|_{0,L} = h''|_{0,L} = 0$) and clamped end points ($h|_{0,L} = h'|_{0,L} = 0$). Notice that, in the latter case, only an approximate solution of the Euler-Lagrange equation (A6) can be found, which is valid in the vicinity of the Euler instability, i.e., for $F \simeq F_c$.

APPENDIX B: LANGEVIN DYNAMICS OF THE MECHANICAL DEGREE OF FREEDOM

For the convenience of the reader, we present a derivation of the Fokker-Planck equation (9). Our derivation is quite general as long as electronic transport is described by rate equations (sequential tunneling). We note that Fokker-Planck equations for nanoelectromechanical systems appeared previously, e.g., in Ref. 14.

We assume that the electromechanical coupling takes the general form $H_c = h(X)n_d$, where h is an arbitrary function of the mode amplitude X. In the classical limit ($\hbar|\omega| \ll k_B T$), and in the sequential tunneling regime ($\hbar\Gamma \ll k_B T$), one can write a Boltzmann equation for the joint probability distribution $\mathcal{P}_n(X,P,t)$ that the resonator is in charge state n ($= 0,1$) and phase-space point (X,P) at time t (Refs. 13,44),

$$\partial_t\mathcal{P}_n = \{\mathcal{H}_n,\mathcal{P}_n\} - (-1)^n\Gamma_{01}(X)\mathcal{P}_0 + (-1)^n\Gamma_{10}(X)\mathcal{P}_1. \tag{B1}$$

The Poisson bracket $\{f,g\} = \partial_X f\,\partial_P g - \partial_P f\,\partial_X g$ describes the classical dynamics of the mechanical degree of freedom on the adiabatic potentials corresponding to the neutral and singly charged states of the quantum dot with Hamiltonian $\mathcal{H}_n = H_{vib} + h(X)n$, where H_{vib} is the vibrational Hamiltonian of Eq. (2). In Eq. (B1), the position-dependent rates for tunneling of electrons in and out of the dot, $\Gamma_{01}(X)$ and $\Gamma_{10}(X)$, respectively, account for the electronic dynamics. Notice that the following derivation does not depend on the specific form of these rates and, hence, on the particular model for the quantum dot which one considers (e.g., metallic or molecular).

Close to the Euler instability, the vibrational mode becomes slow (critical slowing down), and the Poisson bracket in Eq. (B1) can be considered as a small perturbation. If we neglect the Poisson bracket entirely in a first step, the stationary solution of Eq. (B1) reads $\mathcal{P}_0 = \Gamma_{10}\mathcal{P}/\Gamma$, $\mathcal{P}_1 = \Gamma_{01}\mathcal{P}/\Gamma$, with $\mathcal{P} = \mathcal{P}_0 + \mathcal{P}_1$ and $\Gamma = \Gamma_{01} + \Gamma_{10}$. Next, we account for the Poisson bracket perturbatively to leading order by making the ansatz

$$\mathcal{P}_0(X,P,t) = \frac{\Gamma_{10}(X)}{\Gamma(X)}\mathcal{P}(X,P,t) - \delta\mathcal{P}(X,P,t), \tag{B2a}$$

$$\mathcal{P}_1(X,P,t) = \frac{\Gamma_{01}(X)}{\Gamma(X)}\mathcal{P}(X,P,t) + \delta\mathcal{P}(X,P,t). \tag{B2b}$$

In the adiabatic limit in which electronic tunneling is much faster than the vibrational dynamics ($|\omega| \ll \Gamma$), one would then expect that $\delta\mathcal{P}$ is small compared to $\mathcal{P}$ itself. Inserting Eq. (B2) into Eq. (B1), we obtain

$$\partial_t\mathcal{P} = -\frac{P}{m}\partial_X\mathcal{P} - F_{eff}(X)\,\partial_P\mathcal{P} + (\partial_X h)\,\partial_P\delta\mathcal{P} \tag{B3}$$

with the effective force $F_{eff}(X) = -\partial_X H_{vib} - (\partial_X h)\,n_0(X)$ and $n_0(X) = \Gamma_{01}(X)/\Gamma(X)$ the average occupation of the dot for fixed position X, and

$$\begin{aligned}\partial_t\delta\mathcal{P} = {}& \{\mathcal{H}_0,\delta\mathcal{P}\} - \Gamma\delta\mathcal{P} \\ & + (\partial_X h)\left(\frac{\Gamma_{01}\Gamma_{10}}{\Gamma^2}\partial_P\mathcal{P} + \frac{\Gamma_{10}}{\Gamma}\partial_P\delta\mathcal{P}\right) \\ & - \frac{P}{m}\frac{\Gamma_{10}\partial_X\Gamma_{01} - \Gamma_{01}\partial_X\Gamma_{10}}{\Gamma^2}\mathcal{P}.\end{aligned} \tag{B4}$$

So far, Eqs. (B3) and (B4) are exact, and we now make use of the adiabatic limit $\delta\mathcal{P} \ll \mathcal{P}$ to solve them. In this limit, all terms in Eq. (B4) containing $\delta\mathcal{P}$ are negligible compared to those involving $\mathcal{P}$, except for the second term on the right-hand side, which is multiplied by the total tunneling rate $\Gamma \gg |\omega|$. We thus obtain, from Eq. (B4),

$$\delta\mathcal{P} \simeq (\partial_X h)\frac{\Gamma_{01}\Gamma_{10}}{\Gamma^3}\partial_P\mathcal{P} - \frac{P}{m}\frac{\Gamma_{10}\,\partial_X\Gamma_{01} - \Gamma_{01}\,\partial_X\Gamma_{10}}{\Gamma^3}\mathcal{P}. \tag{B5}$$

Inserting this expression into Eq. (B3), we obtain the Fokker-Planck equation (9) (except for the purely extrinsic dissipative and diffusive parts proportional to the damping constant η_e,

which can readily be obtained by coupling the mechanical degree of freedom to a phonon bath) with damping coefficient $\eta(X) = -(\partial_X h)(\partial_X n_0)/\Gamma$ and diffusion constant $D(X) = 2(\partial_X h)^2 n_0(1-n_0)/\Gamma$.

APPENDIX C: CURRENT BLOCKADE FOR A HARMONIC OSCILLATOR LINEARLY COUPLED TO A SET

In this Appendix, we detail the derivation of the Coulomb diamond and the resulting current blockade at low-bias voltage within the zero-temperature mean-field approximation of Sec. IV in the specific case where the resonator coupled to the SET is purely harmonic. We follow and adapt Ref. 7 to the case of a single-level quantum dot, where the average occupation of the island is given by Eq. (22). Specifically, we write the effective potential as

$$v_{\rm eff}(x) = v(x) + \int^x dx'\, n_0(x'), \tag{C1}$$

with

$$v(x) = \frac{v''(\bar{x})}{2}(x-\bar{x})^2. \tag{C2}$$

Introducing $\tilde{x} = x - \bar{x}$ and $\tilde{v}_{\rm g} = v_{\rm g} - \bar{x}$, and using Eq. (22), the condition (21) for dynamical equilibrium at zero temperature reads

$$-v''(\bar{x})\tilde{x} = \begin{cases} 1, & \tilde{x} < \tilde{v}_{\rm g} - \dfrac{v}{2}, \\ \dfrac{1}{2}, & \tilde{v}_{\rm g} - \dfrac{v}{2} \leqslant \tilde{x} \leqslant \tilde{v}_{\rm g} + \dfrac{v}{2}, \\ 0, & \tilde{x} > v_{\rm g} + \dfrac{v}{2}. \end{cases} \tag{C3}$$

In order to solve Eq. (C3), one has to distinguish three cases (see Fig. 10):

(i) $\tilde{v}_{\rm g} > v/2$: In that case, there only exists one solution to Eq. (C3), which corresponds to $n_0 = 1$ and thus is not conducting, $\tilde{x}_1 = -1/v''(\bar{x})$. Therefore, for $\tilde{v}_{\rm g} > v/2$, the system is always nonconducting.

(ii) $|\tilde{v}_{\rm g}| < v/2$: Here, two solutions can coexist: $\tilde{x}_1$ (nonconducting) and $\tilde{x}_{1/2} = -1/2v''(\bar{x})$, which corresponds to $n_0 = 1/2$ and, hence, represents the conducting state of the effective potential. In order for the system to be conducting within our mean-field approximation, this latter solution must be the most stable. This happens whenever $v > v_+ \equiv 2\tilde{v}_{\rm g} + 3/2v''(\bar{x})$.

(iii) $\tilde{v}_{\rm g} < -v/2$: In this last case, an additional solution to Eq. (C3) exists on top of $\tilde{x}_1$ and $\tilde{x}_{1/2}$, namely, $\tilde{x}_0 = 0$, which is not conducting and corresponds to $n_0 = 0$. The conducting solution $\tilde{x}_{1/2}$ is the most stable one if $v > v_+$ and $v > v_- \equiv -2\tilde{v}_{\rm g} - 1/2v''(\bar{x})$.

The apex (defined by $v_+ = v_-$) of the resulting Coulomb diamond sketched in Fig. 10 is thus located at a bias voltage

$$\Delta_v = \frac{1}{2v''(\bar{x})}, \tag{C4}$$

which defines the energy gap below which current cannot flow through the system. The gate voltage corresponding to such a gap is given by $v_{\rm g} = -1/2v''(\bar{x}) + \bar{x}$.

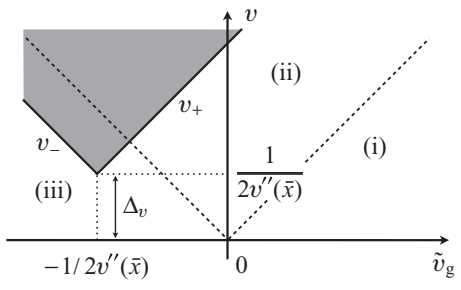

FIG. 10. Sketch of the Coulomb diamond for a SET linearly coupled to a harmonic oscillator, delimited by the solid lines at $v_+ = 2\tilde{v}_{\rm g} + 3/2v''(\bar{x})$ and $v_- = -2\tilde{v}_{\rm g} - 1/2v''(\bar{x})$. The gray area indicates the region where current can flow. The dashed lines indicate the location of the Coulomb diamond without electromechanical coupling ($F_{\rm e} = 0$), delimited by $v = \pm 2\tilde{v}_{\rm g}$, which defines the three regions of the v-$\tilde{v}_{\rm g}$ plane discussed in the text.

APPENDIX D: ANALYTICAL TREATMENT OF THERMAL FLUCTUATIONS

We present here a detailed analytical treatment of the behavior of the current when one only considers thermal fluctuations in the Fokker-Planck equation (15) and compare it to the numerical results presented in Fig. 5 of Sec. V A.

For temperatures much smaller than the gap, the onset of the current with bias voltage has a Fermi-function-like behavior (see dashed and dashed-dotted lines in Fig. 5). This behavior can readily be checked by approximating the effective potential (25) for gate voltages at the apex of the Coulomb diamond [see Eq. (24)] by its zero-temperature expression and by expanding the Boltzmann distribution (19) close to the corresponding minima of that potential. In this limit, the Boltzmann distribution is a superposition of weighted Gaussian peaks centered at these minima (except for $|\delta| \ll \sqrt[3]{\alpha}$ and $x \simeq 0$, where the effective potential is purely quartic in x). For $\tilde{T} \ll \Delta_v$, we find for the current [cf. Eq. (14)]

$$I \simeq \frac{e\Gamma}{4}\left[g\left(\frac{v}{\Delta_v}\right)\exp\left(\frac{\Delta_v - v}{4\tilde{T}}\right) + 1\right]^{-1}, \tag{D1}$$

in good agreement with our numerical results presented in Sec. V A. Far from the Euler instability ($|\delta| \gg \sqrt[3]{\alpha}$), the function $g(z)$ is given by

$$g(z) = \begin{cases} 2, & 0 < z < 2, \\ 0, & z \geqslant 2. \end{cases} \tag{D2}$$

In the vicinity of the instability ($|\delta| \ll \sqrt[3]{\alpha}$), we have

$$g(z) = \begin{cases} \infty, & 0 < z < z_1, \\ 2^{-1/3} + \dfrac{2^{2/3}\Gamma(5/2)}{\sqrt{\pi}}\left(\dfrac{6\Delta_v}{\tilde{T}}\right)^{1/4}, & z_1 \leqslant z < z_2, \\ \dfrac{2^{2/3}\Gamma(5/2)}{\sqrt{\pi}}\left(\dfrac{6\Delta_v}{\tilde{T}}\right)^{1/4}, & z_2 \leqslant z < z_3, \\ 0, & z \geqslant z_3, \end{cases} \tag{D3}$$

where $\Gamma(v)$ denotes the Gamma function, and $z_1 = (2^{5/3}/3 - 1)/(1 - 2^{-1/3})$, $z_2 = 1/3(1 - 2^{-1/3})$, and $z_3 = 1/(1 - 2^{-1/3})$. Notice that the discontinuities in Eqs. (D2) and (D3) are due to the fact that (meta)stable conducting or blocked minima of the effective potential are appearing or disappearing as

one increases the bias voltage. Our approximate result (D1) shows that, at low temperature, the current below the gap is exponentially suppressed as a function of bias voltage.

At higher temperatures, the current starts to be linear in the bias voltage as can be seen from the dotted line in Fig. 5 for $\tilde{T}/\Delta_v = 1$. Indeed, expanding for $\tilde{T} \gg |v_g \pm v/2|$ the current for fixed x, Eq. (13), as well as the Boltzmann distribution (19), we find using Eq. (14)

$$I \simeq C\frac{e\Gamma}{4}\frac{v}{\tilde{T}}, \tag{D4}$$

with

$$C = \frac{\int dy\, f_F(y)\exp\left(\frac{\delta\tilde{T}}{2}y^2 - \frac{\tilde{\alpha}\tilde{T}^3}{4}y^4\right)}{\int dy\, f_F^{-1}(-y)\exp\left(\frac{\delta\tilde{T}}{2}y^2 - \frac{\tilde{\alpha}\tilde{T}^3}{4}y^4\right)}, \tag{D5}$$

to first nonvanishing order in $(v,|v_g|)/\tilde{T}$. For $\tilde{T} \gg \Delta_v$, we find $C \simeq 1/4$ such that

$$I \simeq e\Gamma\frac{eV}{16k_BT}, \tag{D6}$$

which corresponds to the usual high-temperature current in the absence of electromechanical coupling. We have checked that this result is in very good agreement with our numerical calculation of Sec. V A. Of course, when the bias voltage becomes significantly larger than the temperature, the current saturates to its maximal value $I = e\Gamma/4$.

APPENDIX E: STATIONARY SOLUTION OF THE FOKKER-PLANCK EQUATION

We show here that, in the adiabatic limit ($\omega_0/\Gamma \ll 1$) and for weak extrinsic dissipation ($\gamma_e \ll 1$), the stationary solution of the Fokker-Planck equation (15) only depends on the ratio $\frac{\gamma_e}{\omega_0/\Gamma}$. This behavior is exemplified in Fig. 6 where the averaged current flowing through the nanobeam only depends on the latter ratio.

Introducing the new variables

$$E(x,p) = \frac{p^2}{2} + v_{\rm eff}(x), \tag{E1}$$

$$\theta(x,p) = \int_{x_0}^{x}\frac{dx'}{\dot{x}'} = \int_{x_0}^{x}\frac{dx'}{\sqrt{2[E(x,p)-v_{\rm eff}(x')]}}, \tag{E2}$$

with E as the energy of the mechanical degree of freedom and θ as the time along a trajectory in phase space at a given E (x_0 is the initial position of the system for that particular trajectory), the Fokker-Planck equation (15) reads

$$\begin{aligned}\frac{\partial\mathcal{P}}{\partial\tau} = &-\frac{\partial\mathcal{P}}{\partial\theta} + [\gamma(x)+\gamma_e]\left(\mathcal{P} + p^2\frac{\partial\mathcal{P}}{\partial E} + p\frac{\partial\theta}{\partial p}\frac{\partial\mathcal{P}}{\partial\theta}\right)\\ &+\left(\frac{d(x)}{2}+\gamma_e\tilde{T}\right)\left[\frac{\partial\mathcal{P}}{\partial E} + p^2\frac{\partial^2\mathcal{P}}{\partial E^2} + \frac{\partial^2\theta}{\partial p^2}\frac{\partial\mathcal{P}}{\partial\theta}\right.\\ &\left.+\left(\frac{\partial\theta}{\partial p}\right)^2\frac{\partial^2\mathcal{P}}{\partial\theta^2} + 2p\frac{\partial\theta}{\partial p}\frac{\partial^2\mathcal{P}}{\partial E\,\partial\theta}\right].\end{aligned} \tag{E3}$$

Noticing that the current-induced fluctuation and dissipation are both proportional to ω_0/Γ [cf. Eqs. (17) and (18)], we obtain that, for $\omega_0/\Gamma = \gamma_e = 0$, the stationary solution of Eq. (E3), $\partial_\tau\mathcal{P}_{\rm st} = 0$, is independent of θ. This suggests inserting the ansatz

$$\mathcal{P}_{\rm st}(E,\theta) = \bar{\mathcal{P}}_{\rm st}(E) + \delta\mathcal{P}_{\rm st}(E,\theta), \tag{E4}$$

with $\delta\mathcal{P}_{\rm st} \ll \bar{\mathcal{P}}_{\rm st}$ in Eq. (E3). To first order in $(\omega_0/\Gamma,\gamma_e) \ll 1$, we obtain

$$\begin{aligned}0 = &-\frac{\partial\delta\mathcal{P}_{\rm st}}{\partial\theta} + [\gamma(x)+\gamma_e]\left(\bar{\mathcal{P}}_{\rm st} + p^2\frac{\partial\bar{\mathcal{P}}_{\rm st}}{\partial E}\right)\\ &+\left(\frac{d(x)}{2}+\gamma_e\tilde{T}\right)\left(\frac{\partial\bar{\mathcal{P}}_{\rm st}}{\partial E} + p^2\frac{\partial^2\bar{\mathcal{P}}_{\rm st}}{\partial E^2}\right).\end{aligned} \tag{E5}$$

Averaging this equation over one period $\mathcal{T}$ of the motion in phase space and using the periodicity of $\delta\mathcal{P}_{\rm st}$ in θ, we have

$$\begin{aligned}0 = &\left\langle\left(\frac{\gamma(x)}{\gamma_e}+1\right)\left(1+p^2\frac{d}{dE}\right)\right\rangle_E\bar{\mathcal{P}}_{\rm st}\\ &+\left\langle\left(\frac{d(x)}{2\gamma_e}+\tilde{T}\right)\left(1+p^2\frac{d}{dE}\right)\right\rangle_E\frac{d\bar{\mathcal{P}}_{\rm st}}{dE},\end{aligned} \tag{E6}$$

where

$$\langle f(x,p)\rangle_E = \frac{1}{\mathcal{T}}\int_0^{\mathcal{T}}d\theta\, f(x,p). \tag{E7}$$

Since $\gamma(x)$ and $d(x)$ only depend on ω_0/Γ via their prefactors, it is clear, from Eq. (E6), that the stationary solution of the Fokker-Planck equation only depends on ω_0, Γ, and γ_e through the ratio $\frac{\gamma_e}{\omega_0/\Gamma}$.

[1] R. G. Knobel and A. N. Cleland, Appl. Phys. Lett. **81**, 2258 (2002).
[2] R. G. Knobel and A. N. Cleland, Nature (London) **424**, 291 (2003).
[3] A. D. Armour, M. P. Blencowe, and K. C. Schwab, Phys. Rev. Lett. **88**, 148301 (2002).
[4] L. Y. Gorelik, A. Isacsson, M. V. Voinova, B. Kasemo, R. I. Shekhter, and M. Jonson, Phys. Rev. Lett. **80**, 4526 (1998).
[5] F. Pistolesi and R. Fazio, Phys. Rev. Lett. **94**, 036806 (2005).
[6] O. Usmani, Y. M. Blanter, and Y. V. Nazarov, Phys. Rev. B **75**, 195312 (2007).
[7] F. Pistolesi and S. Labarthe, Phys. Rev. B **76**, 165317 (2007).
[8] J. Koch and F. von Oppen, Phys. Rev. Lett. **94**, 206804 (2005).
[9] J. Koch, F. von Oppen, and A. V. Andreev, Phys. Rev. B **74**, 205438 (2006).
[10] R. Leturcq, C. Stampfer, K. Inderbitzin, L. Durrer, C. Hierold, E. Mariani, M. G. Schultz, F. von Oppen, and K. Ensslin, Nat. Phys. **5**, 327 (2009).
[11] D. Mozyrsky, M. B. Hastings, and I. Martin, Phys. Rev. B **73**, 035104 (2006).
[12] F. Pistolesi, Y. M. Blanter, and I. Martin, Phys. Rev. B **78**, 085127 (2008).
[13] A. D. Armour, M. P. Blencowe, and Y. Zhang, Phys. Rev. B **69**, 125313 (2004).

[14]Y. M. Blanter, O. Usmani, and Y. V. Nazarov, Phys. Rev. Lett. **93**, 136802 (2004); **94**, 049904(E) (2005).
[15]C. B. Doiron, W. Belzig, and C. Bruder, Phys. Rev. B **74**, 205336 (2006).
[16]G. A. Steele, A. K. Hüttel, B. Witkamp, M. Poot, H. B. Meerwaldt, L. P. Kouwenhoven, and H. S. J. van der Zant, Science **325**, 1103 (2009).
[17]B. Lassagne, Y. Tarakanov, J. Kinaret, D. Garcia-Sanchez, and A. Bachtold, Science **325**, 1107 (2009).
[18]L. Euler, in *Leonhard Euler's Elastic Curves*, translated and annotated by W. A. Oldfather, C. A. Ellis, and D. M. Brown, reprinted from ISIS, No. 58 XX(1), 1744 (Saint Catherine Press, Bruges).
[19]L. D. Landau and E. M. Lifshitz, *Theory of Elasticity* (Pergamon, Oxford, 1970).
[20]M. R. Falvo, G. J. Harris, R. M. Taylor II, V. Chi, F. P. Brooks Jr., S. Washburn, and R. Superfine, Nature (London) **389**, 582 (1997).
[21]S. M. Carr and M. N. Wybourne, Appl. Phys. Lett. **82**, 709 (2003).
[22]S. M. Carr, W. E. Lawrence, and M. N. Wybourne, Europhys. Lett. **69**, 952 (2005).
[23]D. Roodenburg, J. W. Spronck, H. S. J. van der Zant, and W. J. Venstra, Appl. Phys. Lett. **94**, 183501 (2009).
[24]S. M. Carr, W. E. Lawrence, and M. N. Wybourne, Phys. Rev. B **64**, 220101(R) (2001).
[25]P. Werner and W. Zwerger, Europhys. Lett. **65**, 158 (2004).
[26]V. Peano and M. Thorwart, New J. Phys. **8**, 21 (2006).
[27]S. Savel'ev, X. Hu, and F. Nori, New J. Phys. **8**, 105 (2006).
[28]G. Weick, F. Pistolesi, E. Mariani, and F. von Oppen, Phys. Rev. B **81**, 121409(R) (2010).
[29]A. K. Hüttel, G. A. Steele, B. Witkamp, M. Poot, L. P. Kouwenhoven, and H. S. J. van der Zant, Nano Lett. **9**, 2547 (2009).
[30]Typical parameters for carbon nanotubes of length L and radius R are: $\kappa = 6.3R^3$ [nm] μeV m, $\sigma = 4.2 \times 10^{-15} R$ [nm] kg m^{-1} such that $m = 1.6 \times 10^{-21} R$ [nm] L [μm] kg, $\omega_0 = 610R$ [nm] L^{-2} [μm] MHz, $F_c = 40R^3$ [nm]L^{-2} [μm] pN, and $\alpha = 1.5 \times 10^{27} R^3$ [nm]L^{-5} [μm] eV m^{-4}.
[31]For simplicity, here, we consider spinless fermions. Within the approximations of this paper, the spin would only add a multiplicity factor in the tunneling rates.
[32]E. Mariani and F. von Oppen, Phys. Rev. B **80**, 155411 (2009).
[33]S. Sapmaz, Y. M. Blanter, L. Gurevich, and H. S. J. van der Zant, Phys. Rev. B **67**, 235414 (2003).
[34]W. Izumida and M. Grifoni, New J. Phys. **7**, 244 (2005).
[35]S. Sapmaz, P. Jarillo-Herrero, Y. M. Blanter, C. Dekker, and H. S. J. van der Zant, Phys. Rev. Lett. **96**, 026801 (2006).
[36]K. Flensberg, New J. Phys. **8**, 5 (2006).
[37]More precisely, if $gX^2 n_d/2$ is the intrinsic coupling term (see Ref. 28), we can neglect this term with respect to the linear one if $g \ll F_e^{2/3}\alpha^{1/3}$.
[38]R. Hussein, A. Metelmann, P. Zedler, and T. Brandes, Phys. Rev. B **82**, 165406 (2010).
[39]U. Weiss, *Quantum Dissipative Systems* (World Scientific, Singapore, 1993).
[40]P. Mohanty, D. A. Harrington, K. L. Ekinci, Y. T. Yang, M. J. Murphy, and M. L. Roukes, Phys. Rev. B **66**, 085416 (2002).
[41]C. Seoanez, F. Guinea, and A. H. Castro Neto, EPL **78**, 60002 (2007).
[42]C. Seoanez, F. Guinea, and A. H. Castro Neto, Phys. Rev. B **77**, 125107 (2008).
[43]C. Seoanez, F. Guinea, and A. H. Castro Neto, Phys. Rev. B **76**, 125427 (2007).
[44]F. Elste, G. Weick, C. Timm, and F. von Oppen, Appl. Phys. A **93**, 345 (2008).
[45]Notice that, at equilibrium ($V = 0$), the fluctuating and dissipative parts of the Fokker-Planck equation (9) fulfills the fluctuation-dissipation theorem, i.e., $[D(X)/2 + \eta_e k_B T]/[\eta(X) + \eta_e] = k_B T$.
[46]Notice that, in actual experiments on suspended carbon nanotube quantum dots, the ratio ω_0/Γ is typically very small, of the order of 10^{-2} (see Refs. 16,17,35).
[47]G. Weick *et al.* (unpublished).
[48]P. M. Chaikin and T. C. Lubensky, *Principles of Condensed Matter Physics* (Cambridge University Press, Cambridge, UK, 1995).
[49]At equilibrium ($v = 0$), the effective temperature (26) corresponds to the temperature of the electron reservoirs T, cf. Ref. 45.
[50]Notice, however, that this does not imply a heating of the electron reservoirs as these are considered to be macroscopic. Thus, there is no backaction of the mechanical degree of freedom on the electronic leads, which remain at the equilibrium temperature T.